Journal of Applied Physics

Tuning the p-type doping of GaN over three orders of magnitude via efficient Mg doping during halide vapor phase epitaxy

Cite as: J. Appl. Phys. **132**, 145703 (2022); https://doi.org/10.1063/5.0122292
Submitted: 23 August 2022 • Accepted: 20 September 2022 • Published Online: 14 October 2022

Kazuki Ohnishi, Naoki Fujimoto, Shugo Nitta, et al.

COLLECTIONS

This paper was selected as Featured

ARTICLES YOU MAY BE INTERESTED IN

Process engineering of GaN power devices via selective-area p-type doping with ion implantation and ultra-high-pressure annealing
Journal of Applied Physics **132**, 130901 (2022); https://doi.org/10.1063/5.0107921

Ohmic contact on low-doping-density p-type GaN with nitrogen-annealed Mg
Applied Physics Letters **119**, 242104 (2021); https://doi.org/10.1063/5.0076764

GaN-based power devices: Physics, reliability, and perspectives
Journal of Applied Physics **130**, 181101 (2021); https://doi.org/10.1063/5.0061354

Journal of Applied Physics Special Topics Open for Submissions Learn More

© 2022 Author(s).

Journal of Applied Physics ARTICLE scitation.org/journal/jap

Tuning the p-type doping of GaN over three orders of magnitude via efficient Mg doping during halide vapor phase epitaxy

Cite as: J. Appl. Phys. **132**, 145703 (2022); doi: 10.1063/5.0122292
Submitted: 23 August 2022 · Accepted: 20 September 2022 ·
Published Online: 14 October 2022

View Online

Export Citation

CrossMark

Kazuki Ohnishi,[1,a)] Naoki Fujimoto,[1] Shugo Nitta,[1] Hirotaka Watanabe,[1] Shun Lu,[2] Manato Deki,[3] Yoshio Honda,[1] and Hiroshi Amano[1,3,4]

AFFILIATIONS

[1]Institute of Materials and Systems for Sustainability, Nagoya University, Nagoya 464-8601, Japan
[2]Graduate School of Engineering, Nagoya University, Nagoya 464-8603, Japan
[3]Venture Business Laboratory, Nagoya University, Nagoya 464-8603, Japan
[4]Akasaki Research Center, Nagoya University, Nagoya 464-8603, Japan

[a)]**Author to whom correspondence should be addressed:** k.ohnishi@imass.nagoya-u.ac.jp

ABSTRACT

The precise control of Mg concentration ([Mg]) in p-type GaN layers from 2.3×10^{16} to $2.0 \times 10^{19}\ cm^{-3}$ was demonstrated by halide vapor phase epitaxy (HVPE) on n-type GaN (0001) freestanding substrates. [Mg] in GaN layers could be controlled well by varying the input partial pressure of $MgCl_2$ formed by a chemical reaction between MgO solid and HCl gas under the thermodynamic equilibrium condition. In the sample with [Mg] of $2.0 \times 10^{19}\ cm^{-3}$, a step-bunched surface was observed because the surface migration of Ga adatoms was enhanced by the surfactant effect of Mg atoms. The samples show high structural qualities determined from x-ray rocking curve measurements. The acceptor concentration was in good agreement with [Mg], indicating that almost all Mg atoms act as acceptors. The compensating donor concentrations in the samples were higher than the concentrations of Si, O, and C impurities. We also obtained the Mg acceptor level at a sufficiently low net acceptor concentration of 245 ± 2 meV. These results show that the HVPE method is promising for fabricating GaN vertical power devices, such as n-channel metal–oxide–semiconductor field-effect transistors.

Published under an exclusive license by AIP Publishing. https://doi.org/10.1063/5.0122292

I. INTRODUCTION

The development of p-type conduction in GaN[1,2] led to the great improvement of GaN-based optical[3–5] and electrical devices.[6–8] To obtain p-type conduction in GaN, Mg is generally used as an acceptor. However, it is difficult to achieve a high hole concentration because the ionization energy of Mg acceptors is high.[9–11] In the case of optical devices, such as light-emitting diodes and laser diodes, heavy Mg doping without carrier compensation is required for high-density carrier injection and low contact resistance. On the other hand, the precise wide-range control of Mg doping is required in the fabrication of GaN vertical power devices, which have attracted considerable attention for next-generation power devices owing to the superior material properties of GaN, such as high-breakdown electric field, high electron mobility, and high saturation velocity.[12–14] For example, vertical n-channel metal-oxide-semiconductor field-effect transistors (MOSFETs) require lightly Mg-doped p-type body layers with a Mg concentration ([Mg]) below $10^{18}\ cm^{-3}$ to control the threshold voltage.[15] Moreover, a uniform distribution of Mg atoms in the depth direction is required to prevent punch-through under a high drain bias. Several research groups reported the growth of lightly Mg-doped GaN layers.[15–18] Narita and co-workers reported that the [Mg] of 10^{16}–$10^{20}\ cm^{-3}$ in GaN layers could be precisely controlled and a uniform distribution of Mg atoms in the depth direction could be achieved by using a low Mg doping line equipped with a dilution line and an *in situ* Fourier-transform infrared monitor.[17,18]

GaN vertical power devices and the above-mentioned lightly Mg-doped GaN layers have been grown by metalorganic vapor phase epitaxy (MOVPE).[15–27] Although the doping control method for MOVPE-GaN layers has been investigated, the MOVPE method has an essential problem for growing vertical power

Published under an exclusive license by AIP Publishing

devices. In the MOVPE growth, the incorporation of residual carbon impurity in GaN layers originating from metalorganics is unavoidable. C atoms on nitrogen sites can act as compensating sources in both n- and p-type GaN layers.[28–32] To reduce the residual carbon concentrations ([C]) in GaN layers, the growth at high temperature, high growth pressure, and/or high V/III ratio is effective.[28,33–37] Since the V/III ratio is increased by reducing the partial pressure of III sources, the growth rate is reduced, i.e., there is a trade-off between the V/III ratio and the growth rate. Therefore, it is very difficult to grow thick GaN layers with low [C] in a short time by MOVPE.

In recent years, halide vapor phase epitaxy (HVPE) attracts as a method of growing vertical power devices because thick GaN drift layers with low doping concentration can be grown in a short time. Fujikura and co-workers have reported that high-purity thick GaN drift layers with high electron mobility could be grown by an HVPE system equipped with a quartz-free reactor.[13,38,39] We have fabricated an HVPE-grown GaN vertical p–n junction diode with an ideal avalanche breakdown by establishing the p-type doping method and the guidelines for growing smooth n-type GaN (0001) surfaces.[40–43] In this way, the HVPE method for GaN vertical power devices has been progressively developed. However, the control range of [Mg] by HVPE was on the order of 10^{19}–10^{20} cm^{-3}.[42] Thus, the HVPE method could only be applied to devices that require p$^+$ layers such as p$^+$–n junction diodes. In general, the reduction in the concentration of donor defects is required to obtain p-type conductivity for lightly Mg-doped GaN layers. The introduction of donor defects into p-type body layers also leads to the variation in the threshold voltage of n-channel MOSFETs. Although the tendency of the donor concentrations as a function of [Mg] has been investigated over a wide range for MOVPE-grown p-type GaN layers,[16–18] donor defects in HVPE-grown p-type GaN layers with low [Mg] are not well understood. In order to further develop the HVPE method for vertical power devices, such as n-channel MOSFETs, it is necessary to precisely control [Mg] in GaN layers over a wide range and to achieve a uniform distribution of Mg atoms in the depth direction by HVPE. Moreover, it is important to understand the mechanism of generation of donor defects in HVPE-grown p-type GaN layers with low [Mg]. In this study, we demonstrate the control of [Mg] in a wide range of 10^{16}–10^{19} cm^{-3} in the HVPE-grown p-type GaN layers and characterize them by atomic force microscopy (AFM), x-ray diffraction, and Hall-effect measurements. For Mg doping in the HVPE method, it has been reported that $MgCl_2$ is a key precursor for the thermodynamic analysis.[44] We can control [Mg] in GaN layers over a wide range by varying only the input $MgCl_2$ partial pressure.

II. EXPERIMENTAL PROCEDURE

N-type GaN (0001) freestanding substrates with a threading dislocation density on the order of 10^6 cm^{-2} grown by HVPE were used. The off-cut angles and carrier concentrations of these substrates were 0.55° toward the *m*-axis and on the order of 10^{18} cm^{-3}, respectively. These substrates were introduced to a horizontal HVPE reactor. This HVPE system has two source reaction zones and one growth zone. A Ga melt and a MgO solid can be heated into the two separated source reaction zones. Our HVPE system has been described in detail in Ref. 41. GaCl, which was formed by the reaction between the Ga melt and HCl gas, and NH_3 gas were used as Ga and N precursors, respectively. The Ga melt was set to the source reaction zone heated at 850–900 °C. In this temperature range, GaCl was fully formed by the reaction between the Ga melt and HCl gas. Approximately 200-nm-thick Si-doped n-type GaN layers were grown on GaN freestanding substrates, followed by the growth of 12-μm-thick Mg-doped GaN layers. $SiCl_4$ was used as the dopant gas for the growth of n-type GaN layers. For Mg doping, the $MgCl_2$ gas formed by the reaction between the MgO solid and HCl gas was used. The chemical reaction between the MgO solid and HCl gas has been clarified by the thermodynamic analysis.[44] According to Ref. 44, the $MgCl_2$ partial pressure increases by MgO temperature and the input HCl flow rate. Also, the formation rate of $MgCl_2$ increases with increasing MgO temperature. To precisely control [Mg] in GaN layers over a wide range, the MgO solid temperature and the input HCl flow rate were changed for low and high Mg-doping regimes.

For the low Mg-doping regime, i.e., [Mg] < 10^{18} cm^{-3}, [Mg] was controlled by changing the MgO solid temperature from 600 to 800 °C at a constant input HCl flow rate of 0.2 SCCM. In this regime, the low $MgCl_2$ partial pressure is required. However, the control of low HCl flow rate is difficult. Hence, the low $MgCl_2$ partial pressure was kept by changing the formation rate of $MgCl_2$, i.e., changing the MgO temperature.

In contrast, for high Mg-doping regime, i.e., [Mg] ≥ 10^{18} cm^{-3}, [Mg] was controlled by changing the input HCl flow rate from 0.4 to 4 SCCM at a constant MgO temperature of 900 °C. In this regime, the high $MgCl_2$ partial pressure is essential. To obtain high $MgCl_2$ partial pressure, the formation rate of $MgCl_2$ was increased by high MgO temperature.

Mg-doped GaN layers were grown in a temperature range of 1060–1065 °C and at a pressure of 1 atm. The input HCl partial pressure in the Ga melt and the NH_3 partial pressure were set to 1.3×10^{-3} and 1.3×10^{-1} atm, respectively. A mixture of H_2 and N_2 gases was used as the carrier gas and the input $H_2/(H_2 + N_2)$ ratio was 0.23. The growth rate of Mg-doped GaN layers was set to 30 μm/h. The impurity concentrations of Mg-doped GaN layers were characterized by secondary ion mass spectrometry (SIMS). The surface morphology was observed using AFM (SII 5500 M). To investigate the structural properties of samples, x-ray rocking curve measurements were carried out with an x-ray diffractometer (Rigaku Smartlab). The Cu-Kα_1 x ray with a four-bounced Ge (440) monochromator (beam size: 0.5×10 mm^2) was used as an incident beam. To characterize the electrical properties of p-type GaN layers, van der Pauw Hall-effect measurement was performed using a ToyoResitest8300 system under an AC magnetic field with an amplitude of 0.5 T. For Hall-effect measurements, 7×7-mm^2-squares Hall devices were prepared. These devices were annealed at 700 °C for 5 min in nitrogen ambient to remove hydrogen atoms. Then, Ni/Au ohmic electrodes were deposited at four corners of these devices. For Hall devices with [Mg] < 10^{19} cm^{-3}, diffused Mg-containing contact layers annealed in nitrogen ambient were formed under ohmic electrodes to obtain ohmic contacts.[45,46] Details on how to form contact layers and their properties have been described in Refs. 45 and 46.

Published under an exclusive license by AIP Publishing

III. RESULTS AND DISCUSSION

The SIMS depth profile of [Mg] in Mg-doped GaN layers grown at various input partial pressure ratios of $MgCl_2$ and GaCl R_{Mg} $[=P^0_{MgCl_2}/(P^0_{MgCl_2}+P^0_{GaCl})$, where P^0_i is the input partial pressure of chemical species i] is shown in Fig. 1(a). $P^0_{MgCl_2}$ was estimated from results in Ref. 44. Mg atoms were uniformly doped in depth directions. Figure 1(b) shows the average [Mg] as a function of R_{Mg}. A linear relationship between [Mg] and R_{Mg} in the double logarithmic plot was found, indicating that the chemical reaction between MgO solid and HCl gas proceeds under the thermodynamic equilibrium condition. Thus, Mg doping over a wide [Mg] range can be controlled well by varying only the input partial pressure of $MgCl_2$ formed by the chemical reaction between MgO solid and HCl gas.

In order to observe surface morphologies of the Mg-doped GaN layers, the AFM analysis was performed. Figure 2 shows 5×5-μm^2-squares AFM images of as-grown Mg-doped GaN surfaces. In the Mg-doped GaN surfaces with [Mg] of 2.3×10^{16}–1.8×10^{18} cm^{-3}, the step and terrace structures were clearly observed. The root-mean-square (RMS) roughnesses of these samples were 0.18–0.20 nm, indicating that the smooth surfaces were formed. On the other hand, bunched steps were observed in the sample with [Mg] of 2.0×10^{19} cm^{-3}. The RMS roughness was 1.0 nm, which was five times larger than those of the samples with [Mg] of 2.3×10^{16}–1.8×10^{18} cm^{-3}. Mg atoms function as a surfactant for the growth of GaN, and Mg doping can promote the surface migration of Ga adatoms.[47] Heavy Mg doping is considered to promote surface migration and a surface with bunched steps is formed during the HVPE growth of GaN (0001) layers.

Structural properties of Mg-doped GaN layers were investigated by XRC measurement. Figures 3(a) and 3(b) show GaN 0004 and $10\bar{1}2$ XRC reflection peaks of Mg-doped GaN layers with [Mg] of 2.3×10^{16}–2.0×10^{19} cm^{-3}, respectively. As a reference, XRC reflection peaks of a 15-μm-thick n-type GaN layer with Si concentration ([Si]) of 3×10^{16} cm^{-3} were also shown. The full width at half maximum (FWHM) values of both the GaN 0004 and $10\bar{1}2$ XRC reflection peaks of the samples were between 23 and 32 arcs. These values were very close to those of the reference sample, indicating that HVPE-grown Mg-doped GaN layers with [Mg] in the range of 2.3×10^{16}–2.0×10^{19} cm^{-3} have high structural quality.

In order to characterize the electrical properties of Mg-doped GaN layers with [Mg] of 2.3×10^{16}–2.0×10^{19} cm^{-3}, the Hall-effect measurements were performed. For measuring the hole concentration p and hole mobility, the Hall scattering factor of unity was assumed. To measure the carrier concentration of a sample by Hall-effect measurement, it is important to determine the effective thickness of the conductive layer, which is different from the physical thickness of a Mg-doped GaN layer. We estimated the surface and interface depletion widths of the Mg-doped GaN layers. In the estimation of the surface depletion width, the surface pinning level with an energy level of 1.7 eV above the valence band maximum was assumed.[48] In the Mg-doped sample with [Mg] of 2.3×10^{16} cm^{-3}, the surface and interface depletion widths toward the Mg-doped GaN layer were estimated to be 0.57 and 0.38 μm, respectively. Thus, we measured p in the sample with [Mg] of

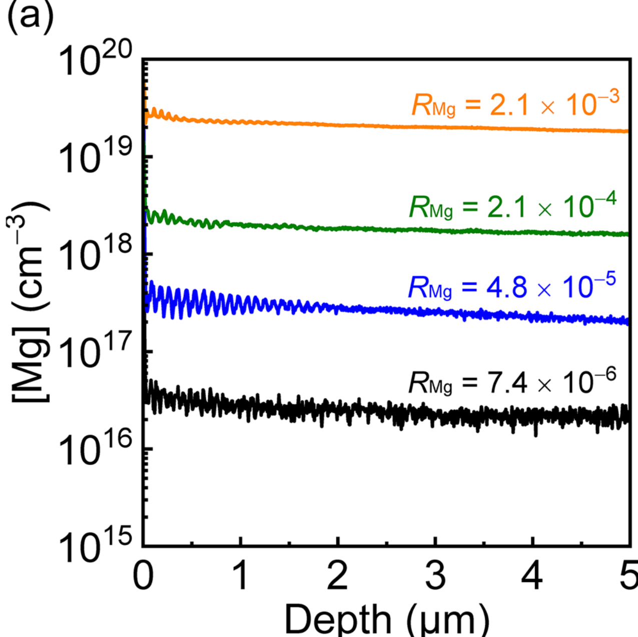

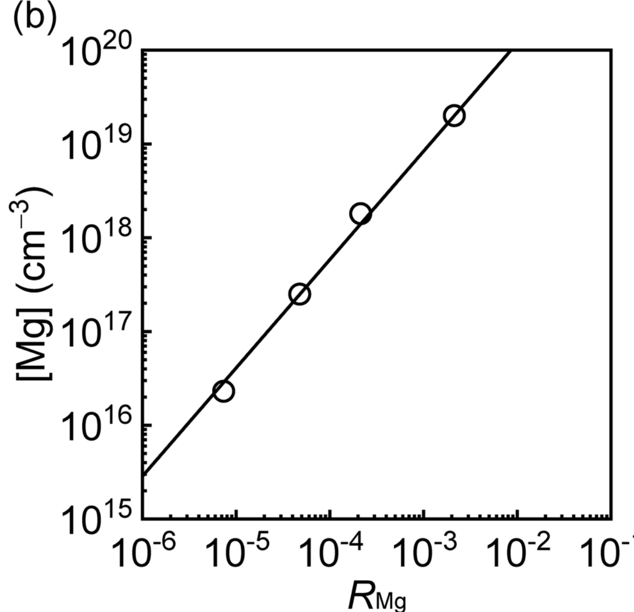

FIG. 1. (a) SIMS depth profile of [Mg] for Mg-doped GaN layers with various R_{Mg} values and (b) average [Mg] in Mg-doped GaN layers as a function of $R_{Mg}[=P^0_{MgCl_2}/(P^0_{MgCl_2}+P^0_{GaCl})]$. The input $MgCl_2$ partial pressure was estimated from results in Ref. 44.

2.3×10^{16} cm^{-3} by assuming the effective thickness of 11 μm. For [Mg] in the samples higher than 2.5×10^{17} cm^{-3}, on the other hand, the sum of the surface and interface depletion widths toward the Mg-doped GaN layer was smaller than 0.2 μm. Hence, we can

Published under an exclusive license by AIP Publishing

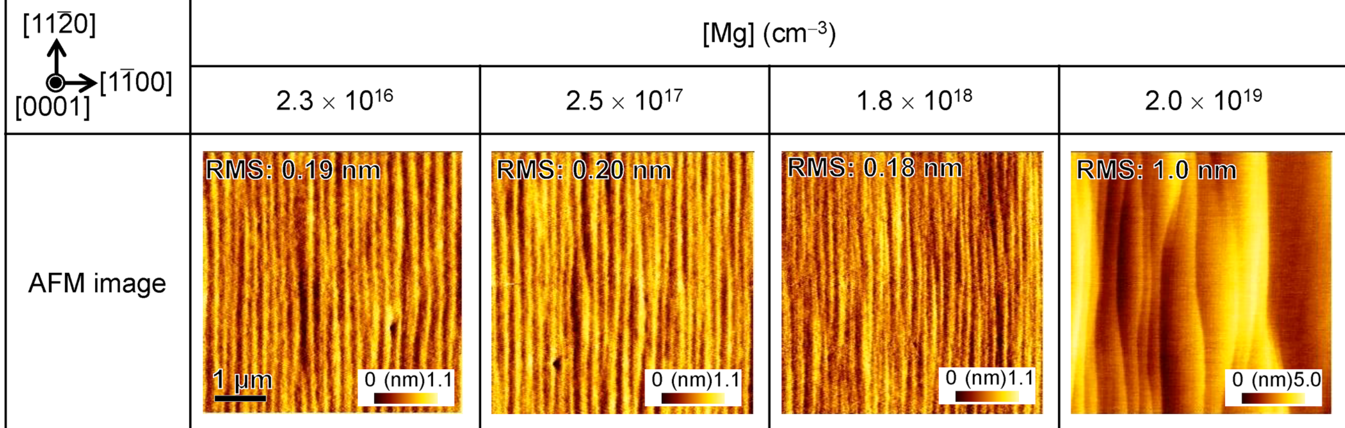

FIG. 2. 5×5-μm^2-squares AFM images of Mg-doped GaN surfaces with [Mg] of 2.3×10^{16}–2.0×10^{19} cm^{-3}.

neglect the effect of surface and interface depletion widths on the samples with $[\mathrm{Mg}] \geq 2.5 \times 10^{17}$ cm^{-3}, i.e., the effective thicknesses of the samples were equal to this physical thickness of 12 μm. All samples show p-type conduction at room temperature. The Arrhenius plots of p of the samples are shown in Fig. 4. The hole concentration increased with [Mg]. To analyze p, a fitting analysis was performed by considering the semiconductor statistics and the charge neutrality with the fitting parameters of the acceptor concentration N_a, compensating donor concentration N_d, and the ionization energy ΔE_a. The theoretical analysis formula can be expressed as

$$p + N_d = \frac{N_a}{1 + \frac{gp}{N_v}\exp\left(\frac{\Delta E_a}{k_B T}\right)}, \tag{1}$$

where k_B and T are the Boltzmann coefficient and temperature in Kelvin, respectively. The degeneracy factor g of the valence band was 4. N_v is the effective density of states in the valence band and is expressed as

$$N_v = N_{v,\ 300\,K}\left(\frac{T}{300}\right)^{3/2}. \tag{2}$$

Here, $N_{V,300\,K}$, which is the effective density of states in the valence band at 300 K, was assumed as 7.3×10^{19} cm^{-3} reported in Ref. 16. The fitting curves for all samples were in good agreement with the experimental hole concentrations in the samples with $[\mathrm{Mg}] \leq 1.8 \times 10^{18}$ cm^{-3}. In contrast, the experimental hole concentration differed from the theoretical fitting curve at a temperature lower than 170 K in the sample with [Mg] of 2.0×10^{19} cm^{-3}. In this region, the hopping or impurity band conduction was predominant.[16,49]

Figure 5 shows the obtained ionization energy as a function of the net acceptor concentration $N_a - N_d$. ΔE_a decreases with increasing net acceptor concentration owing to the Coulomb potential of ionized acceptors as[50,51]

$$\Delta E_a = E_{a0} - f\,(N_a - N_d)^{1/3}, \tag{3}$$

where E_{a0} is the Mg acceptor level at a sufficiently low net acceptor concentration and f is a constant. The fitted line was in good agreement with the obtained ΔE_a value. The value of f was experimentally obtained to be $(2.6 \pm 0.1) \times 10^{-5}$ meV cm. This value was close to the theoretical value of 3.3×10^{-5} meV cm obtained on the basis of the relative dielectric constant of 9.5.[9,52] The extrapolated value from the fitted line was 245 ± 2 meV, corresponding to E_{a0}. The obtained E_{a0} value was within the reported experimental value of 245 ± 25 meV[11] and close to the theoretical value of 260 meV.[10] This indicates that the p-type conduction of the samples with [Mg] of 2.3×10^{16}–2.0×10^{19} cm^{-3} fitted in the range of the framework of Eq. (1) is due to the ionization of Mg acceptors.

The obtained N_a and N_d values as functions of [Mg] in the Mg-doped GaN layers are shown in Fig. 6. The solid line shows that N_a is equal to [Mg]. We found that the N_a value was close to [Mg], indicating that almost all Mg atoms incorporated into GaN layers act as acceptors. The obtained N_d value increased with [Mg]. This tendency is consistent with the results of MOVPE-grown Mg-doped GaN layers.[17] Table I shows [Mg], [C], [Si], and O concentrations ([O]) measured by SIMS and the obtained N_a and N_d values for Mg-doped GaN layers. Si, O, and C impurities were most likely the donor sources for GaN. Although the incorporation of O impurity was a concern because of the use of MgO solid as a Mg source, [O] in Mg-doped GaN layers was lower than 1.2×10^{16} cm^{-3} at most (for [Mg] of 2.0×10^{19} cm^{-3}). This indicates that the unintentional [O] originating from MgO was about three orders of magnitude lower than [Mg]. [Si] in Mg-doped GaN layers, which was $(5–7) \times 10^{15}$ cm^{-3}, was independent of [Mg] because of the incorporation of Si impurity from the quartz HVPE reactor. Additionally, [C] in the samples was lower than the detection limit (3×10^{15} cm^{-3}) because of the use of the carbon-free III source. In the samples with [Mg] values of 2.3×10^{16} and

Published under an exclusive license by AIP Publishing

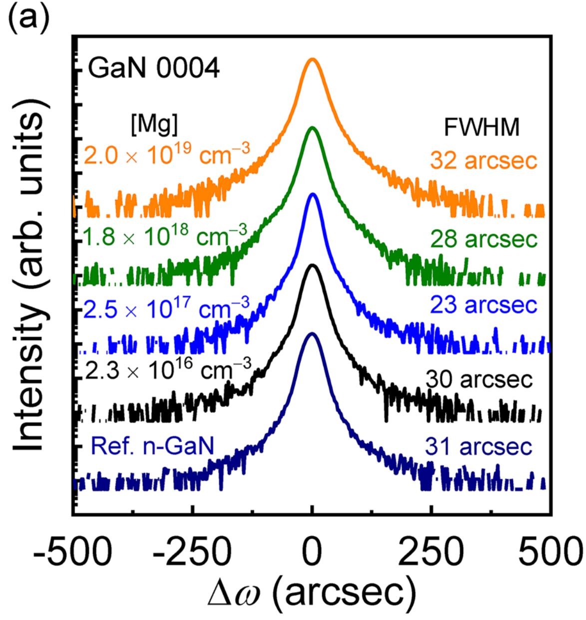

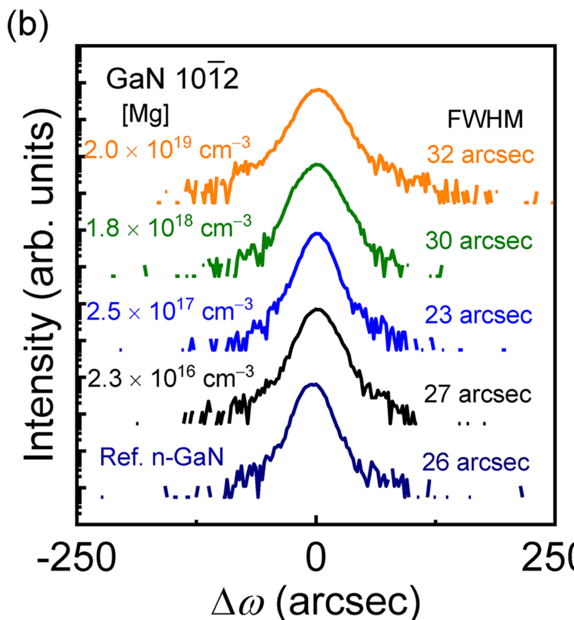

FIG. 3. (a) GaN 0004 and (b) GaN $10\bar{1}2$ XRC reflection peaks of Mg-doped GaN layers with [Mg] of 2.3×10^{16}–2.0×10^{19} cm^{-3}. As a reference, XRC peaks of the n-type GaN layer with [Si] of 3×10^{16} cm^{-3} are shown.

2.5×10^{17} cm^{-3}, [Si] values were 44% and 23% of N_d values, respectively. Moreover, the sum of [Si], [O], and [C] was much lower than the N_d value in the samples with $[Mg] \geq 1.8 \times 10^{18}$ cm^{-3}. Hence, in addition to Si, O, and C impurities, other donors, such as nitrogen vacancies[53] and/or hydrogen atoms,[10] might be the origin of compensating donors. To reduce N_d values in Mg-doped p-type GaN layers grown by HVPE, the reduction in a residual [Si] and/or the concentration of point defects is essential. To reduce [Si] and the concentration of point defects in GaN layers, several studies have been carried out. Fujikura *et al.* reported that unintentionally doped GaN layers with [Si] lower than 5×10^{14} cm^{-3} could be grown by using a quartz-free HVPE reactor.[38] Reddy *et al.* reported that the concentration of point defects in MOVPE-grown GaN layers could be reduced by chemical potential control, i.e.,

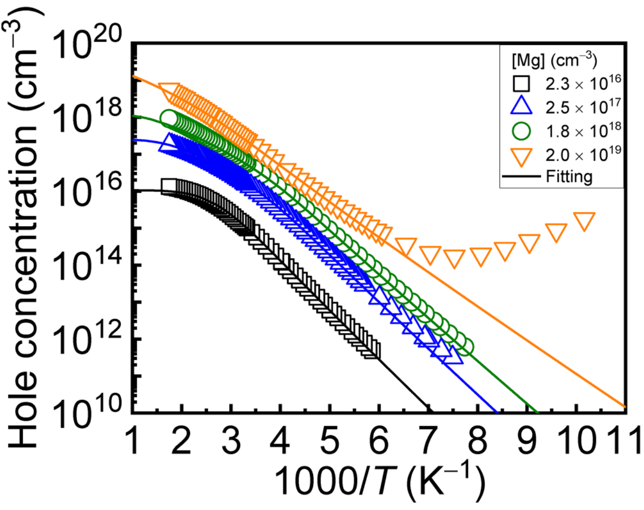

FIG. 4. Arrhenius plots of the hole concentrations of Mg-doped GaN layers with [Mg] of 2.3×10^{16}–2.0×10^{19} cm^{-3} obtained by Hall-effect measurements.

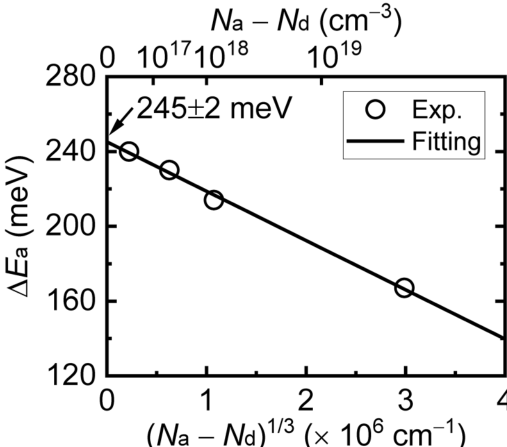

FIG. 5. Ionization energy as a function of net acceptor concentration. Experimental data are plotted as circles. The solid line shows the fitted result obtained by Eq. (3). The extrapolated ionization energy is 245 ± 2 meV, indicating that the depth of the Mg acceptor level at a sufficiently low net acceptor concentration.

Published under an exclusive license by AIP Publishing

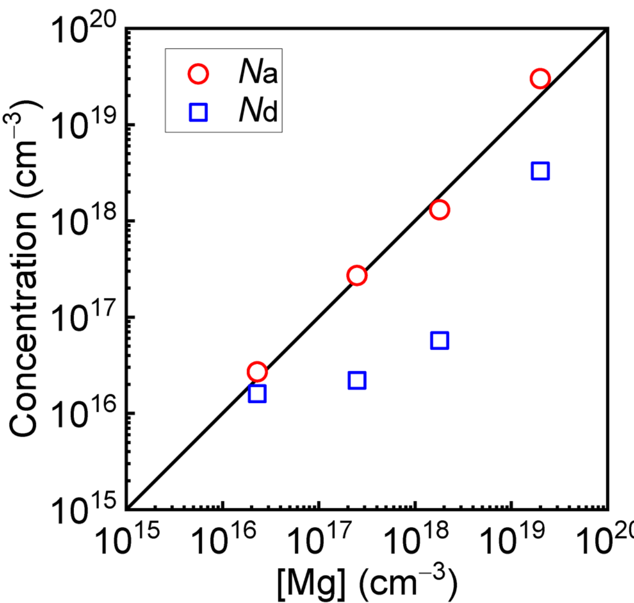

FIG. 6. Obtained N_a and N_d values as functions of [Mg] in Mg-doped GaN layers. N_a and N_d were estimated by Hall-effect measurements. The solid line shows that N_a is equal to [Mg].

increasing the formation energy of point defects by varying the growth condition, as expressed by supersaturation.[37] Accordingly, it will be effective to utilize the quartz-free HVPE reactor and chemical potential control for further reduction in N_d in p-type GaN layers grown by HVPE.

Then, we focused on the hole mobilities in Mg-doped GaN layers with [Mg] of 2.3×10^{16}–2.0×10^{19} cm^{-3}. Figure 7(a) shows the temperature dependence of hole mobilities in the samples. In the sample with [Mg] of 2.0×10^{19} cm^{-3}, the hole mobility increased from 100 to 170 K and subsequently decreased with increasing temperature. The hopping or impurity band conduction was predominant in the region lower than 170 K, resulting in low hole mobility. On the other hand, hole mobility decreased with increasing temperature in the samples with [Mg] $\leq 1.8 \times 10^{18}$ cm^{-3}. Additionally, the tendency of temperature dependence of hole mobility was similarly observed in these samples. This implies that

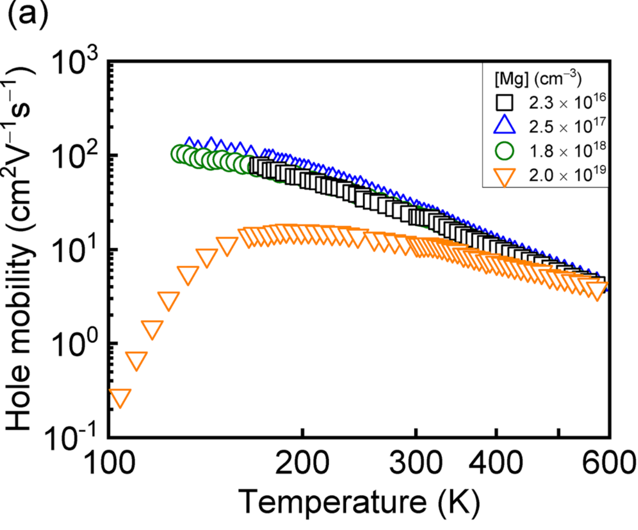

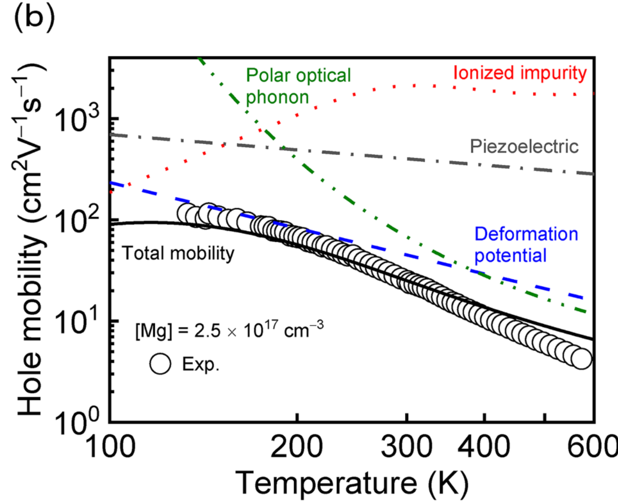

FIG. 7. (a) Temperature dependence of hole mobilities in Mg-doped GaN layers with [Mg] of 2.3×10^{16}–2.0×10^{19} cm^{-3}. (b) Experimental and calculated hole mobilities in the sample with [Mg] of 2.5×10^{17} cm^{-3}. For calculation, the effective hole mass of $2.04m_0$, corresponding to $N_{V,300\,K} = 7.3 \times 10^{19}$ cm^{-3}, reported in Ref. 16 was used.

TABLE I. Summary of impurity concentrations, N_a, and N_d of the Mg-doped GaN layers. [Mg], [Si], [O], and [C] were measured by SIMS. N_a and N_d values were obtained by Hall-effect measurements.

SIMS				Hall-effect		
[Mg] (cm^{-3})	[Si] (cm^{-3})	[O] (cm^{-3})	[C] (cm^{-3})	N_a (cm^{-3})	N_d (cm^{-3})	N_d/N_a (%)
2.3×10^{16}	7×10^{15}	$<6 \times 10^{15}$	$<3 \times 10^{15}$	2.7×10^{16}	1.6×10^{16}	59
2.5×10^{17}	5×10^{15}	$<6 \times 10^{15}$	$<3 \times 10^{15}$	2.7×10^{17}	2.2×10^{16}	8
1.8×10^{18}	6×10^{15}	$<6 \times 10^{15}$	$<3 \times 10^{15}$	1.3×10^{18}	5.7×10^{16}	4
2.0×10^{19}	6×10^{15}	1.2×10^{16}	$<3 \times 10^{15}$	3.0×10^{19}	3.3×10^{18}	11

Published under an exclusive license by AIP Publishing

the scattering mechanism was common in the samples with $[Mg] \leq 1.8 \times 10^{18}\,cm^{-3}$. We quantitatively analyzed hole mobility by considering conduction within the valence band using Matthiessen's rule for the individual scattering mechanism reported by Kyle *et al.*[54] The following scattering mechanisms were considered: ionized impurity scattering, neutral impurity scattering, deformation potential scattering, piezoelectric scattering, and polar optical phonon scattering. Single-charged donors and acceptors were assumed to calculate ionized impurity scattering. The effect of dislocation scattering on the threading dislocation density is very small on the order of $10^6\,cm^{-2}$.[32,54] Thus, the dislocation scattering can be neglected in this study. Figure 7(b) shows the experimental and calculated hole mobilities in the sample with [Mg] of $2.5 \times 10^{17}\,cm^{-3}$. The hole mobility limited by neutral impurity scattering was higher than $10^5\,cm^2\,V^{-1}\,s^{-1}$; thus, it was not plotted in this figure. The calculated total mobility showed a reasonable agreement with the experimental mobility. Additionally, the calculated mobilities were close to the experimental values in the samples with [Mg] values of 2.3×10^{16} and $1.8 \times 10^{18}\,cm^{-3}$ (not shown here). Thus, the experimental hole mobilities for the samples with $[Mg] \leq 1.8 \times 10^{18}\,cm^{-3}$ can be theoretically explained by the individual scattering mechanism within the valence band.

IV. CONCLUSIONS

The precise control of [Mg] in p-type GaN layers over a wide range of 2.3×10^{16}–$2.0 \times 10^{19}\,cm^{-3}$ with high crystal qualities has been achieved by HVPE. The Mg doping profiles in p-type GaN layers were uniform in the depth direction. [Mg] can be controlled well by varying R_{Mg}, which results from the formation of $MgCl_2$ by the reaction between MgO solid and HCl gas under the thermodynamic equilibrium condition. Smooth surfaces with step and terrace structures were clearly observed in the samples with $[Mg] \leq 1.8 \times 10^{18}\,cm^{-3}$. In contrast, a step-bounced surface was observed in the sample with [Mg] of $2.0 \times 10^{19}\,cm^{-3}$ because the surface migration of Ga adatoms was enhanced owing to the surfactant effect of Mg atoms. The XRC FWHM values of the GaN 0004 and $10\bar{1}2$ reflection peaks of all samples were very narrow in the range of 23–32 arcs. The N_a values in all HVPE-grown p-type GaN layers were close to [Mg] in GaN layers, indicating that almost all Mg atoms incorporated into GaN layers act as acceptors. The Mg acceptor level at a sufficiently low doping concentration was 245 ± 2 meV, which was very close to reported values. N_d increased with [Mg] in the samples. Regarding the origin of compensating donors in HVPE-grown p-type GaN layers, not only the donor impurities of Si, O, and C but also other donors, such as nitrogen vacancies and/or hydrogen atoms, are considered. In the Mg-doped GaN layers with $[Mg] \leq 1.8 \times 10^{18}\,cm^{-3}$, the temperature dependence of hole mobility was theoretically explained by considering the individual scattering mechanism within the valence band. On the other hand, the hole mobility dropped below 170 K in the heavily Mg-doped GaN layer with [Mg] of $2.0 \times 10^{19}\,cm^{-3}$. This implies that the hopping or impurity band conduction was predominant in the region below 170 K. The present results show that the Mg doping over a wide range of [Mg] by HVPE can be promising for fabricating GaN vertical power devices, such as p–n junction diodes and MOSFETs.

ACKNOWLEDGMENTS

This research was supported by MEXT-Program for Creation of Innovative Core Technology for Power Electronics Program under Grant No. JPJ009777. We would like to thank Ms. Kiyoko Ban for supporting this research.

AUTHOR DECLARATIONS

Conflict of Interest

The authors have no conflicts to disclose.

Author Contributions

Kazuki Ohnishi: Conceptualization (lead); Formal analysis (lead); Investigation (lead); Methodology (lead); Visualization (lead); Writing – original draft (lead). **Naoki Fujimoto:** Investigation (supporting); Writing – review & editing (equal). **Shugo Nitta:** Investigation (supporting); Project administration (equal); Resources (equal); Writing – review & editing (equal). **Hirotaka Watanabe:** Investigation (supporting); Writing – review & editing (equal). **Shun Lu:** Investigation (supporting); Writing – review & editing (equal). **Manato Deki:** Investigation (supporting); Writing – review & editing (equal). **Yoshio Honda:** Project administration (equal); Resources (equal); Writing – review & editing (equal). **Hiroshi Amano:** Project administration (equal); Resources (equal); Supervision (lead); Writing – review & editing (equal).

DATA AVAILABILITY

The data that support the findings of this study are available from the corresponding author upon reasonable request.

REFERENCES

[1] H. Amano, M. Kito, K. Hiramatsu, and I. Akasaki, Jpn. J. Appl. Phys. **28**, L2112 (1989).
[2] S. Nakamura, T. Mukai, M. Senoh, and N. Iwasa, Jpn. J. Appl. Phys. **31**, L139 (1992).
[3] I. Akasaki and H. Amano, Jpn. J. Appl. Phys. **45**, 9001 (2006).
[4] S. Nakamura, T. Mukai, and M. Senoh, Appl. Phys. Lett. **64**, 1687 (1994).
[5] S. Nagahama, N. Iwasa, M. Senoh, T. Matsushita, Y. Sugimoto, H. Kiyoku, T. Kozaki, M. Sano, H. Matsumura, and H. Umemoto, Jpn. J. Appl. Phys. **39**, L647 (2000).
[6] T. Kachi, Jpn. J. Appl. Phys. **53**, 100210 (2014).
[7] H. Amano, Y. Baines, E. Beam, M. Borga, T. Bouchet, P. R. Chalker, M. Charles, K. J. Chen, N. Chowdhury, R. Chu, C. De Santi, M. M. De Souza, S. Decoutere, L. Di Cioccio, B. Eckardt, T. Egawa, P. Fay, J. J. Freedsman, L. Guido, O. Häberlen, G. Haynes, T. Heckel, D. Hemakumara, P. Houston, J. Hu, M. Hua, Q. Huang, A. Huang, S. Jiang, H. Kawai, D. Kinzer, M. Kuball, A. Kumar, K. B. Lee, X. Li, D. Marcon, M. März, R. McCarthy, G. Meneghesso, M. Meneghini, E. Morvan, A. Nakajima, E. M. S. Narayanan, S. Oliver, T. Palacios, D. Piedra, M. Plissonnier, R. Reddy, M. Sun, I. Thayne, A. Torres, N. Trivellin, V. Unni, M. J. Uren, M. Van Hove, D. J. Wallis, J. Wang, J. Xie, S. Yagi, S. Yang, C. Youtsey, R. Yu, E. Zanoni, S. Zeltner, and Y. Zhang, J. Phys. D: Appl. Phys. **51**, 163001 (2018).
[8] T. Oka, Jpn. J. Appl. Phys. **58**, SB0805 (2019).
[9] W. Götz, R. S. Kern, C. H. Chen, H. Liu, D. A. Steigerwald, and R. M. Fletcher, Mater. Sci. Eng. B **59**, 211 (1999).
[10] J. L. Lyons, A. Janotti, and C. G. Van de Walle, Phys. Rev. Lett. **108**, 156403 (2012).

Published under an exclusive license by AIP Publishing

[11] S. Brochen, J. Brault, S. Chenot, A. Dussaigne, M. Leroux, and B. Damilano, Appl. Phys. Lett. **103**, 032102 (2013).
[12] T. Maeda, T. Narita, S. Yamada, T. Kachi, T. Kimoto, M. Horita, and J. Suda, J. Appl. Phys. **129**, 185702 (2021).
[13] H. Fujikura, T. Konno, T. Kimura, Y. Narita, and F. Horikiri, Appl. Phys. Lett. **117**, 012103 (2020).
[14] J. Kolník, İ. H. Oğuzman, K. F. Brennan, R. Wang, P. P. Ruden, and Y. Wang, J. Appl. Phys. **78**, 1033 (1995).
[15] S. Takashima, K. Ueno, H. Matsuyama, T. Inamoto, M. Edo, T. Takahashi, M. Shimizu, and K. Nakagawa, Appl. Phys. Express **10**, 121004 (2017).
[16] M. Horita, S. Takashima, R. Tanaka, H. Matsuyama, K. Ueno, M. Edo, T. Takahashi, M. Shimizu, and J. Suda, Jpn. J. Appl. Phys. **56**, 031001 (2017).
[17] T. Narita, N. Ikarashi, K. Tomita, K. Kataoka, and T. Kachi, J. Appl. Phys. **124**, 165706 (2018).
[18] T. Narita, H. Yoshida, K. Tomita, K. Kataoka, H. Sakurai, M. Horita, M. Bockowski, N. Ikarashi, J. Suda, T. Kachi, and Y. Tokuda, J. Appl. Phys. **128**, 090901 (2020).
[19] Y. Saitoh, K. Sumiyoshi, M. Okada, T. Horii, T. Miyazaki, H. Shiomi, M. Ueno, K. Katayama, M. Kiyama, and T. Nakamura, Appl. Phys. Express **8**, 081001 (2010).
[20] W. Li, K. Nomoto, M. Pilla, M. Pan, X. Gao, D. Jena, and H. G. Xing, IEEE Trans. Electron Devices **64**, 1635 (2017).
[21] M. Kanechika, M. Sugimoto, N. Soejima, H. Ueda, O. Ishiguro, M. Kodama, E. Hayashi, K. Itoh, T. Uesugi, and T. Kachi, Jpn. J. Appl. Phys. **46**, L503 (2007).
[22] T. Oka, T. Ina, Y. Ueno, and J. Nishii, Appl. Phys. Express **8**, 054101 (2015).
[23] H. Hatakeyama, K. Nomoto, N. Kaneda, T. Kawano, T. Mishima, and T. Nakamura, IEEE Electron Device Lett. **32**, 1674 (2011).
[24] K. Nomoto, B. Song, Z. Hu, M. Zhu, M. Qi, N. Kaneda, T. Mishima, T. Nakamura, D. Jena, and H. G. Xing, IEEE Electron Device Lett. **37**, 161 (2016).
[25] I. C. Kizilyalli, T. Prunty, and O. Aktas, IEEE Electron Device Lett. **36**, 1073 (2015).
[26] H. Ohta, K. Hayashi, F. Horikiri, M. Yoshino, T. Nakamura, and T. Mishima, Jpn. J. Appl. Phys. **57**, 04FG09 (2018).
[27] H. Ohta, N. Asai, F. Horikiri, Y. Narita, T. Yoshida, and T. Mishima, IEEE Electron Device Lett. **41**, 123 (2020).
[28] N. Sawada, T. Narita, M. Kanechika, T. Uesugi, T. Kachi, M. Horita, T. Kimoto, and J. Suda, Appl. Phys. Express **11**, 041001 (2018).
[29] J. L. Lyons, A. Janotti, and C. G. Van de Walle, Appl. Phys. Lett. **97**, 152108 (2010).
[30] D. O. Demchenko, I. C. Diallo, and M. A. Reshchikov, Phys. Rev. Lett. **110**, 087404 (2013).
[31] J. L. Lyons, A. Janotti, and C. G. Van de Walle, Phys. Rev. B **89**, 035204 (2014).
[32] T. Narita, K. Tomita, Y. Tokuda, T. Kogiso, M. Horita, and T. Kachi, J. Appl. Phys. **124**, 215701 (2018).
[33] G. Parish, S. Keller, S. P. Denbaars, and U. K. Mishra, J. Electron. Mater. **29**, 15 (2000).
[34] D. D. Koleske, A. E. Wickenden, R. L. Henry, and M. E. Twigg, J. Cryst. Growth **242**, 55 (2002).
[35] G. Piao, K. Ikenaga, Y. Yano, H. Tokunaga, A. Mishima, Y. Ban, T. Tabuchi, and K. Matsumoto, J. Cryst. Growth **456**, 137 (2016).
[36] T. Ciarkowski, N. Allen, E. Carlson, R. McCarthy, C. Youtsey, J. Wang, P. Fay, J. Xie, and L. Guido, Materials **12**, 2455 (2019).
[37] P. Reddy, S. Washiyama, F. Kaess, R. Kirste, S. Mita, R. Collazo, and Z. Sitar, J. Appl. Phys. **122**, 245702 (2017).
[38] H. Fujikura, T. Konno, T. Yoshida, and F. Horikiri, Jpn. J. Appl. Phys. **56**, 085503 (2017).
[39] H. Fujikura, K. Hayashi, F. Horikiri, Y. Narita, T. Konno, T. Yoshida, H. Ohta, and T. Mishima, Appl. Phys. Express **11**, 045502 (2018).
[40] K. Ohnishi, S. Kawasaki, N. Fujimoto, S. Nitta, H. Watanabe, Y. Honda, and H. Amano, Appl. Phys. Lett. **119**, 152102 (2021).
[41] K. Ohnishi, Y. Amano, N. Fujimoto, S. Nitta, Y. Honda, and H. Amano, Appl. Phys. Express **13**, 061007 (2020).
[42] K. Ohnishi, Y. Amano, N. Fujimoto, S. Nitta, H. Watanabe, Y. Honda, and H. Amano, J. Cryst. Growth **566–567**, 126173 (2021).
[43] K. Ohnishi, N. Fujimoto, S. Nitta, H. Watanabe, Y. Honda, and H. Amano, J. Cryst. Growth **592**, 126749 (2022).
[44] T. Kimura, K. Ohnishi, Y. Amano, N. Fujimoto, M. Araidai, S. Nitta, Y. Honda, H. Amano, Y. Kangawa, and K. Shiraishi, Jpn. J. Appl. Phys. **59**, 088001 (2020).
[45] S. Lu, M. Deki, J. Wang, K. Ohnishi, Y. Ando, T. Kumabe, H. Watanabe, S. Nitta, Y. Honda, and H. Amano, Appl. Phys. Lett. **119**, 242104 (2021).
[46] J. Wang, S. Lu, W. Cai, T. Kumabe, Y. Ando, Y. Liao, Y. Honda, Y.-H. Xie, and H. Amano, IEEE Electron Device Lett. **43**, 150 (2022).
[47] V. Ramachandran, R. M. Feenstra, W. L. Sarney, L. Salamanca-Riba, J. E. Northup, L. T. Romano, and D. W. Greve, Appl. Phys. Lett. **75**, 808 (1999).
[48] D. Segev and C. G. Van de Walle, J. Cryst. Growth **300**, 199 (2007).
[49] P. Kozodoy, H. Xing, S. P. DenBaars, U. K. Mishra, A. Saxler, R. Perrin, S. Elhamri, and W. C. Mitchel, J. Appl. Phys. **87**, 1832 (2000).
[50] G. L. Pearson and J. Bardeen, Phys. Rev. **75**, 865 (1949).
[51] P. P. Debye and E. M. Conwell, Phys. Rev. **93**, 693 (1954).
[52] K. Karch, J.-M. Wagner, and F. Bechstedt, Phys. Rev. B **57**, 7043 (1998).
[53] Q. Yan, A. Janotti, M. Scheffler, and C. G. Van de Walle, Appl. Phys. Lett. **100**, 142110 (2012).
[54] E. C. H. Kyle, S. W. Kaun, P. G. Burke, F. Wang, Y.-R. Wu, and J. S. Speck, J. Appl. Phys. **115**, 193702 (2014).

Published under an exclusive license by AIP Publishing